EPJ D
Atomic, Molecular, Optical and Plasma Physics
EPJ.org
your physics journal

Eur. Phys. J. D (2014) 68: 360 DOI: 10.1140/epjd/e2014-50312-3

Radiation pressure force on cold rubidium atoms due to excitation to a non-cooling hyperfine level

Gordana Kregar, Neven Šantić, Damir Aumiler and Ticijana Ban

edp sciences
Società Italiana di Fisica
Springer

Eur. Phys. J. D (2014) 68: 360
DOI: 10.1140/epjd/e2014-50312-3

THE EUROPEAN PHYSICAL JOURNAL D

Regular Article

Radiation pressure force on cold rubidium atoms due to excitation to a non-cooling hyperfine level

Gordana Kregar[1], Neven Šantić[1,2], Damir Aumiler[1], and Ticijana Ban[1,a]

[1] Institute of Physics, Bijenička cesta 46, 10000 Zagreb, Croatia
[2] Department of Physics, University of Zagreb, Bijenička cesta 32, 10002 Zagreb, Croatia

Received 18 April 2014 / Received in final form 28 July 2014
Published online 1 December 2014 –

Abstract. We study the radiation pressure force exerted on cold ^{87}Rb atoms captured in a magneto-optical trap (MOT) due to resonant excitation of atoms into the non-cooling $5P_{1/2}(F_e = 2)$ hyperfine level. We measure the fractional excited population for different MOT parameters such as cooling laser detuning and power, and empirically test the applicability of the Optical Bloch Equations for describing cold atoms in the MOT. We use the effective saturation intensity parameter which enables simple calculation of the fractional excited state population in a multi-level system using a two-level model, and apply it for the radiative force modeling. This approach provides a valuable tool for optical manipulation experiments.

1 Introduction

Radiation pressure force is a result of the interaction of laser light with atoms, allowing it to modify the motion of an atom, i.e. its momentum and kinetic energy. This optical force is the basis for laser cooling and trapping of atoms, a technique which enables the production of sufficiently dense cold atomic samples. New classes of matter like Bose-Einstein Condensate (BEC) [1], degenerate Fermi [2] and Bose-Fermi [3] gases were realized from cold atomic and/or molecular samples leading to one of the most promising and productive fields of contemporary research.

The mechanical action of the radiation pressure force on cold atoms has been the topic of our recent research. In our recent work, we have investigated the radiative force on cold rubidium atoms induced by femtosecond pulse train (frequency comb) excitation [4]. We have shown that the frequency comb can in some geometry and for some parameters probe the boundary between the quantum (internal dynamics) and the classical (center-of-mass motion) worlds, which can complicate the calculation of the force induced by the frequency comb. Furthermore, we have demonstrated a novel scheme for creating synthetic Lorentz force for cold atomic gases via Doppler effect and radiation pressure [5]. The key idea is to use multi-level structure of the atoms and orthogonal continuous-wave (cw) laser fields in conjunction with the Doppler effect resulting in velocity dependent perpendicular radiation pressure force on atoms. This cold atom manipulation scheme opens the possibility to mimic classical charged gases in magnetic fields. However, quantitative and qualitative assessment of the radiation pressure force is crucial for understanding and predicting the experimental results of this new cold atom all-optical manipulation schemes, which ultimately provided the motivation for this work.

In general, the radiation pressure force depends on a number of parameters such as: detuning of the laser frequency from the resonant transition (influenced by Doppler and Zeeman effects), transition probabilities, saturation, laser intensities, optical pumping, and laser beam alignment and profile [6]. However, modeling of the radiation force is usually based on the solutions of the Optical Bloch Equations (OBEs) for a two-level atom interacting with a single frequency (cw) laser field; and on the Ehrenfest theorem [7]. This approximation is satisfactory in the case of excitation of optically closed transition, but it is not straightforward in the case of multi-level atomic system interacting with multi-frequency laser fields such as cold atoms in MOT.

The force from absorption followed by spontaneous emission on a two-level atom can be written as [7]:

$$\mathbf{F}_{sp} = \hbar \mathbf{k} \Gamma \rho_{ee}, \tag{1}$$

where $\hbar\mathbf{k}$ is the photon momentum, Γ is the rate of the process (excited state population decay rate). ρ_{ee} is the probability for the atoms to be in the excited state given by:

$$\rho_{ee} = \frac{A s_0}{1 + s_0 + (2\Delta/\Gamma)^2}, \tag{2}$$

where s_0 is the saturation parameter, Δ is the laser detuning from the atomic resonance frequency, and A is a constant equal to 0.5 for two-level atom. $s_0 = I/I_s$

[a] e-mail: ticijana@ifs.hr

with I being the laser intensity, and I_s the saturation intensity [8]:

$$I_s = \frac{\pi h c \Gamma}{3\lambda^3}. \quad (3)$$

Here h is the Planck constant, c is the speed of light, and λ is the wavelength of the atomic transition.

Applying equation (3) to ^{87}Rb $5S_{1/2} \rightarrow 5P_{3/2}$, D2 resonance transition at 780 nm, $\Gamma/2\pi = 6.07$ MHz gives $I_s = 1.67$ mW/cm^2. This value is valid for a two-level atom interacting with a single frequency field. In cold atom experiments, however, it is necessary to consider more complex phenomena such as the effects of optical pumping, multiple scattering, laser intensity imperfection, and beam shadowing. The fraction of excited ^{87}Rb atoms in the MOT was directly measured in the work of Shah et al. [9] using a charge transfer technique. They showed that it can be accurately estimated knowing only the trapping laser intensity and detuning. For low saturation parameter, $s_0 < 1.25$, the simple model given by equation (2) was used to fit the measured fractions. They obtained saturation intensity for ^{87}Rb $5S_{1/2}(F_g = 2) \rightarrow 5P_{3/2}(F_e = 3)$ cooling transition of $2I_s = 9.2 \pm 1.7$ mW/cm^2, which is 2.75 times larger than the value calculated from equation (3). Similar results were obtained by Dinneen et al. [10], where the population of excited ^{87}Rb atoms in the MOT is measured using a trap loss technique. Effective saturation intensity of ^{87}Rb $5S_{1/2}(F_g = 2) \rightarrow 5P_{3/2}(F_e = 3)$, D2 resonance transition was also measured in [11], using absorption imaging technique (ballistically expanded cloud, i.e. MOT is switched off). Even in this condition, the authors have measured the correction factor of $\alpha^* = 2.12 \pm 0.1$ to the two-level saturation intensity.

From the above, it is clear that there is a need for accurate determination of the saturation intensity I_s in multi-level atom interacting with multi-frequency laser fields, which is a necessary prerequisite for predicting the fractional excited state population and therefore the radiation force exerted on atoms. Moreover, accurate determination of the fractional excited state population is crucial for the determination of the number of cold atoms in optical traps [12,13], cold atom collision processes [14], determination of the absolute photoionization cross section [10], population transfer [15], etc. It uniquely describes the interaction of cold atoms with their environment such as their excitation by different laser fields.

To our knowledge, there are no determination of the excited state fractional population and saturation intensity I_s for other hyperfine transitions in cold rubidium atoms captured in MOT. This hinders theoretical modeling of other physical parameters which are related to these transitions; such as radiative force, collision cross sections, photoassociation rates, etc.

We therefore devote the first part of our paper to the measurements of the fractional excited state population in the non-cooling $P_{1/2}(F_e = 2)$ hyperfine level for cold ^{87}Rb atoms in the MOT. For this purpose, we introduce an additional low-intensity probe laser in the MOT and measure the associated laser induced fluorescence (LIF) at 795 nm for different MOT parameters and probe intensities. We also employ a theoretical approach based on solving OBEs (for five-level atoms interacting with three laser fields – cooling, repumper, and probe lasers) to model the fractional excited state population in the non-cooling level. We validate qualitatively the model by comparing its results with the measured LIF. Finally, we use the model results to introduce the effective saturation intensity parameter for ^{87}Rb D1 resonance transition. The effective saturation intensity parameter I_s^{eff}, together with equation (2), enables the reduction of the complex multi-level system perturbed by multiple lasers to the simple two-level atom model.

In the second part of the paper, we investigate the radiation pressure force on cold ^{87}Rb atoms induced by the probe laser. We use the I_s^{eff} to model the force, while simultaneously measuring the probe-induced radiative force using an approach based on cloud imaging. The technique is accurate, simple, and robust; and can easily be implemented in variety of experimental situations. The comparison between experiment and theory is very good, confirming the applicability of our approach to the radiative force modeling.

2 Experiment

The experiment was performed on ^{87}Rb atoms cooled and trapped in a vapor-loaded magneto-optical trap (MOT). The trap is set up in the standard $\sigma^+\sigma^-$ retro-reflected configuration, with beam diameters of 2 cm. Cooling and repumper lasers are external cavity diode lasers (ECDL, Toptica DL100 laser systems) delivering total powers of 50 mW and 10 mW, respectively. The cooling laser is typically 2−3 linewidths red-detuned from the ^{87}Rb D2 $F_g = 2 \rightarrow F_e = 3$ hyperfine transition. The repumper laser is in resonance with the ^{87}Rb D2 $F_g = 1 \rightarrow F_e = 2$ hyperfine transition, thus keeping most of the population in the $5S_{1/2}(F_g = 2)$ ground level. The quadrupole magnetic field is provided by a pair of anti-Helmholtz coils. The number of atoms in the trap is deduced by measuring the cloud fluorescence with a calibrated photodiode [16]. The cloud density distribution is measured by imaging the cloud fluorescence onto a CCD chip.

The trap spring constant κ is obtained from a transient oscillation method [17]. We have measured the trajectory of the atomic cloud after the additional external force is switched off, and the cloud returns to the original MOT center. The atomic motion in MOT is given by a damped harmonic oscillator model. The trap frequencies and damping coefficients for different MOT parameters are obtained from fitting procedure. Uncertainties of κ measurements include uncertainties of cooling and repumper laser power and detuning, and of magnetic field gradient (due to quadrupole coils heating).

In typical experimental conditions (13 G/cm-axial magnetic field gradient, $2\pi \times 12$ MHz-cooling laser detuning), we obtain a cloud of (0.9 ± 0.1) mm radius that

contains about 8×10^8 ^{87}Rb atoms, characterized by a trap spring constant $\kappa = (1.3 \pm 0.2) \times 10^{-19}$ N/m.

Such a cloud of cold rubidium atoms was the starting point for two kinds of experiments; one related to the measurements of the fractional excited state population and the other to the radiative force measurements.

In the first part, the cold rubidium atoms are excited by a focused probe laser beam adjusted in a retro-reflected configuration, and propagating almost colinearly with one of the cooling beams. The probe laser is a low power (maximum power 10 mW) external cavity diode laser (ECDL, Toptica DL 100), locked to the ^{87}Rb D1 $5S_{1/2}(F_g = 2) \rightarrow 5P_{1/2}(F_e = 2)$ hyperfine transition. Its power is controlled by an acousto-optic modulator (AOM). In order to avoid the frequency shift of the probe beam after passing through the AOM, the experimental scheme developed in reference [18] was used. The probe beam spatial profile is measured using a beam profiler. Measured beam profile intensity distribution fits a Gaussian function, with halfwidth equal to HWHM $= (0.34 \pm 0.05)$ mm. The probe laser power is changed within the $(0-100)$ μW range, corresponding to the $(0-27)$ mW/cm^2 intensity range. Laser induced fluorescence (LIF) from the excited $5P_{1/2}(F_e = 2)$ level at 795 nm was measured with a spectrometer (Shamrock sr-303i), equipped with a holographic grating (1800 gr/mm) and a CCD camera (Andor iDus 420). Fluorescence was collected by a lens and imaged onto the entrance slit of the spectrometer with a slit width of 100 μm and a 40 ms exposure time.

In Figure 1 we show simultaneous LIF measurements at 780 nm and 795 nm for different probe laser intensities I_p. Here I_p represents spatially averaged and total intensity of the probe beam, obtained by dividing the total probe power by the area within the probe beam radius. Error bars are obtained from ten independent LIF measurements. LIF at 780 nm is a result of spontaneous emission from the $5P_{3/2}(F_e = 3)$ excited level, populated by the cooling laser, and can be used for the estimation of the total number of cold atoms in MOT. LIF at 795 nm is a result of spontaneous emission from the $5P_{1/2}(F_e = 2)$ excited level, populated by the probe laser. Considering that the cooling laser is red detuned (i.e. it is positioned at the slope of the Lorentz function that describes the excited state population), the number of the excited atoms in $5P_{3/2}(F_e = 3)$ level changes significantly with the frequency dither of the cooling laser, thus increasing uncertainty of LIF measurement at 780 nm compared to the LIF at 795 nm. By inspection of Figure 1 it is clear that the number of cold atoms in the MOT remains constant during the measurements of the fractional $5P_{1/2}(F_e = 2)$ excited level population; i.e. there is no trap loss of atoms associated with the probe beam excitation due to heating, optical pumping and mechanical action. The conservation of the number of atoms in the MOT is ensured by the small probe laser beam diameter (almost three times smaller than the radius of the cloud), low probe power, and optimized overlaping of the counterpropagating probe beams.

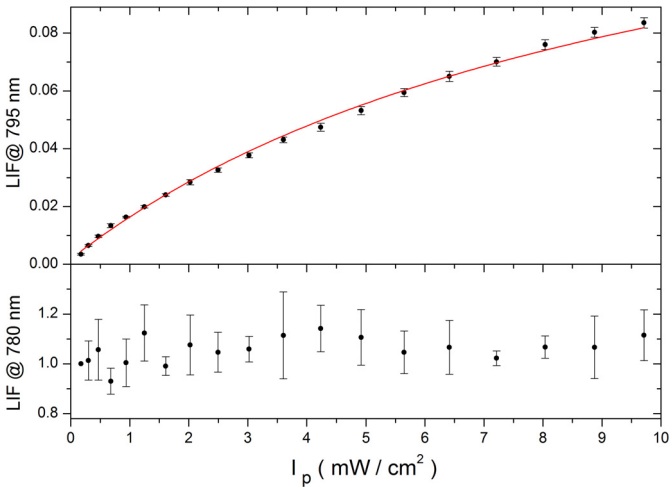

Fig. 1. LIF measured simultaneously at 780 nm and 795 nm showing constant number of cold atoms in the MOT during the measurements of the fractional $5P_{1/2}(F_e = 2)$ excited level population. LIF signals are normalized to the LIF intensity at 780 nm without the probe laser. Error bars are obtained from ten independent LIF measurements.

In the second part of the experiment, we have measure the probe-induced radiative force using an approach based on cloud imaging. We have used the same probe laser but with beam diameter around 2.5 mm (in order to induce uniform radiation force across the cloud). The fluorescence intensity distribution of the cold cloud is imaged by a calibrated CMOS camera for different probe beam intensities. The images are then processed and the position of the center of mass (CM) of the cold atomic cloud is determined. Under the radiation pressure force of the probe laser, the CM of the cloud is displaced by Δx in the direction of the probe beam. The probe laser force is balanced by the MOT force, which for cold atoms ($v \approx 0$, and therefore the dissipative part of the force can be neglected) gives:

$$\mathbf{F}_{probe} = \kappa \, \Delta x. \tag{4}$$

The technique was recently used for the measurement of the radiation pressure force on cold ^{87}Rb atoms induced by the femtosecond pulse train [4]. Also, a variation of this technique was used in [19] to determine the spring constant.

3 Optical Bloch equations for cold atoms in the MOT excited by the probe laser

Standard density matrix formalism was utilized to model the $5P_{1/2}(F_e = 2)$ excited level fractional population in different MOT conditions; i.e. different cooling laser detuning and power.

Our model system, shown in Figure 2, is a five-level ^{87}Rb atom interacting with three independent continuous-wave laser fields (cooling E_c, repumper E_r, and probe E_p). The cooling laser couples $5S_{1/2}(F_g = 2) - 5P_{3/2}(F_e = 3)$

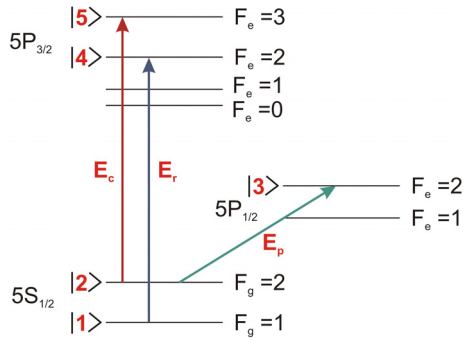

Fig. 2. Hyperfine energy level scheme relevant for theoretical modeling. The arrows indicate cooling, repumper and excitation laser frequencies.

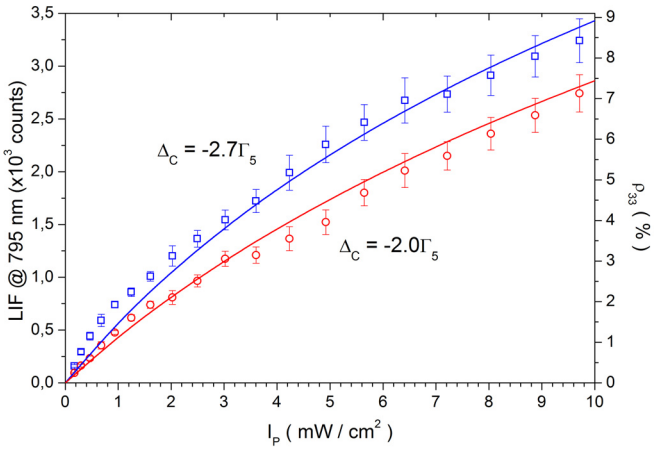

Fig. 3. Comparison of the measured (LIF at 795 nm, points, left y-axis) and calculated (ρ_{33}, solid lines, right y-axis) fractional $5P_{1/2}(F_e = 2)$ level populations as a function of the probe laser intensity, for two cooling laser detunings. Error bars are obtained from three independent LIF measurements.

levels ($|2\rangle - |5\rangle$), repumper laser couples $5S_{1/2}(F_g = 1) - 5P_{3/2}(F_e = 2)$ levels ($|1\rangle - |4\rangle$), and probe laser couples $5S_{1/2}(F_g = 2) - 5P_{1/2}(F_e = 2)$ levels ($|2\rangle - |3\rangle$).

The Hamiltonian of the system, $\hat{H} = \hat{H}_0 + \hat{H}_{int}$, consists of two parts; the free atom Hamiltonian $\hat{H}_0$ and the interaction Hamiltonian $\hat{H}_{int}$. The latter describes the interaction of the atom with three independent laser fields, $\hat{H}_{int} = H_{25} + H_{14} + H_{23}$. In the dipole approximation parts of the interaction Hamiltonian can be written as $H_{25} = -\mu_{25}\mathcal{E}_c(t)$, $H_{14} = -\mu_{14}\mathcal{E}_r(t)$ and $H_{23} = -\mu_{23}\mathcal{E}_p(t)$, where μ_{25}, μ_{14}, and μ_{23} are transition dipole moments of the relevant transitions numbered according to Figure 2 and calculated from reference [20].

Temporal evolution of the system is given by the density matrix equations of motion [21]:

$$\begin{aligned}\frac{\partial\rho_{nm}}{\partial t} &= \frac{-i}{\hbar}\left[\hat{H},\hat{\rho}\right]_{nm} - \gamma_{nm}\rho_{nm}, \quad (n \neq m),\\ \frac{\partial\rho_{nn}}{\partial t} &= \frac{-i}{\hbar}\left[\hat{H},\hat{\rho}\right]_{nn} - \sum_{m(E_m<E_n)} \Gamma_{mn}\rho_{nn}\\ &\quad + \sum_{m(E_m>E_n)} \Gamma_{nm}\rho_{mm}, \end{aligned} \tag{5}$$

where the subscripts n, m refer to the hyperfine levels numbered from the lowest to highest energy level (see Fig. 2). Γ_{nm} gives the population decay rate from level m to level n, while γ_{nm} is the damping rate of the ρ_{nm} coherence given by:

$$\gamma_{nm} = \frac{1}{2}(\Gamma_n + \Gamma_m). \tag{6}$$

Here Γ_n and Γ_m denote the total population decay rates of level n and m. In our system $\Gamma_1 = \Gamma_2 = 0$, $\Gamma_3 = 2\pi \times 5.75$ MHz, $\Gamma_4 = \Gamma_5 = 2\pi \times 6.06$ MHz [8]. Γ_{nm} are calculated from Γ_n and Γ_m following Fermi's golden rule [20].

The usual method to solve the system of equation (5) is to invoke the rotating-wave approximation and introduce laser electric fields $\mathcal{E}_c(t) = E_c e^{i\omega_c t}$, $\mathcal{E}_r(t) = E_r e^{i\omega_r t}$, and $\mathcal{E}_p(t) = E_p e^{i\omega_p t}$, together with the slowly varying coherences $\sigma_{25} = \rho_{25}e^{-i\omega_c t}$, $\sigma_{14} = \rho_{14}e^{-i\omega_r t}$, and $\sigma_{23} = \rho_{23}e^{-i\omega_p t}$. Here, ω_c, ω_r, and ω_p are cooling, repumper, and probe laser frequencies defined as $\omega_c = \omega_{25} + \Delta_c$, $\omega_r = \omega_{14}$, and $\omega_p = \omega_{23}$, where ω_{25}, ω_{14}, and ω_{23} correspond to the ^{87}Rb $5S_{1/2}(F_g = 2) \rightarrow 5P_{3/2}(F_e = 3)$, $5S_{1/2}(F_g = 1) \rightarrow 5P_{3/2}(F_e = 2)$, and $5S_{1/2}(F_g = 2) \rightarrow 5P_{1/2}(F_e = 2)$ hyperfine transition frequencies, respectively [8]. E_c, E_r, and E_p are the amplitudes of the cooling, repumper and probe laser fields.

Stationary solutions for atomic populations and coherences are obtained from the resulting set of coupled differential equations. Starting with fixed MOT parameters (E_c, E_r, and Δ_c) we calculated the fractional $5P_{1/2}(F_e = 2)$ level population, ρ_{33}, for different probe field amplitudes, E_p. The dependence of the ρ_{33} upon intensity of the probe laser is obtained using relation $I = \frac{cn\epsilon_o}{2}E^2$, where c is the speed of light, n is the index of refraction, and ϵ_o is the permittivity of vacuum.

4 Fractional excited state population of the non-cooling level

In Figure 3 we present the comparison of measured LIF at 795 nm (points, given in counts, left y-axis) and calculated ρ_{33} fractional $5P_{1/2}(F_e = 2)$ level population (solid lines, right y-axis) as a function of the probe laser intensity, for two detunings of the cooling laser, $\Delta_c = -2.0\Gamma_5$ and $-2.7\Gamma_5$. The calculations are performed for the cooling and repumper laser intensities of 13 mW/cm^2 and 0.6 mW/cm^2, respectively, which correspond to their experimental values (I_c and I_r are given by the sum of the average intensities of the six beams). Measured LIF at 795 nm agrees qualitatively with the calculated fractional $5P_{1/2}(F_e = 2)$ level populations (ρ_{33}). LIF is proportional to ρ_{33}, however no scaling between the LIF counts and the calculated excited state populations shown in Figure 3 has been made. ρ_{33} increases with increasing the probe beam intensity, and saturates for larger intensities. For a given probe laser intensity, fractional $5P_{1/2}(F_e = 2)$ level population increases with detuning of the cooling laser.

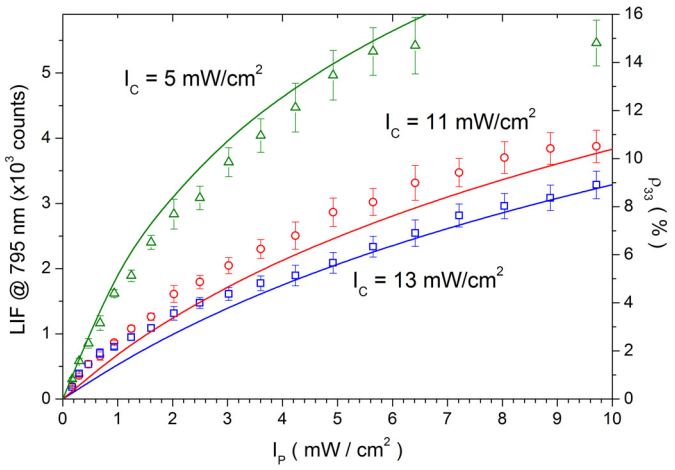

Fig. 4. Comparison of the measured (LIF at 795 nm, points) and calculated (ρ_{33}, solid lines) fractional $5P_{1/2}(F_e = 2)$ level populations as a function of the probe laser intensity, for three cooling laser powers. Error bars are obtained from three independent LIF measurements.

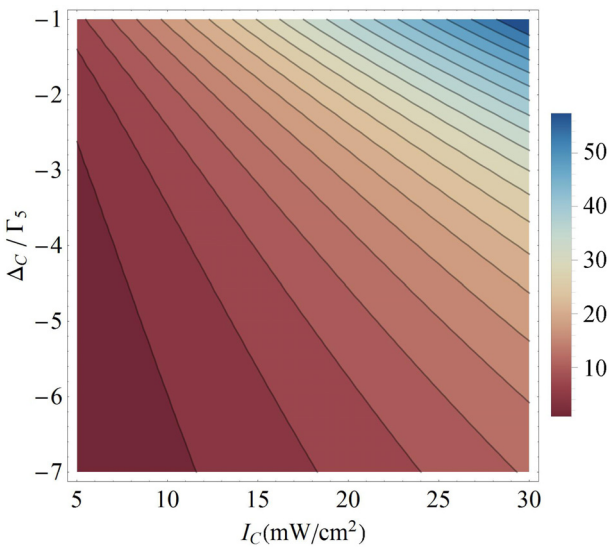

Fig. 5. Density plot of calculated I_s^{eff} as a function of cooling laser detuning and power. The values of I_s^{eff} shown by the color bar are given in mW/cm^2.

The number of cold atoms in MOT (without probe laser) depends on the MOT parameters, i.e. cooling laser detuning, cooling and repumper laser powers. Consequently, for different MOT parameters different LIF signals at 780 nm are expected (without the probe). In order to qualitatively compare experiment and theory (OBEs are calculated for fixed number of the cold atoms in MOT), this change in the number of cold atoms in MOT for different MOT parameters has to be compensated. Therefore all measured LIF signals at 795 nm for different MOT parameters are corrected with the factor corresponding to the rate of change of the number of cold atoms in MOT (without probe laser). We should also note that the fluorescence is measured in the retroreflected probe laser configuration (producing a standing wave), with the probe beam smaller than the cold atom cloud. The atoms therefore experience a range of probe intensities that results from both the standing wave and the Gaussian probe beam profile. In the calculated populations (shown in Figs. 3 and 4) we performed averaging of the results over the distribution of intensities present in the experiment. Alternatively, one could also simply do the calculations at an average probe intensity value (which actually turns out to be a reasonably accurate first approximation), but this approach is generally not valid under conditions where saturation is important.

The comparison of measured LIF at 795 nm and calculated fractional $5P_{1/2}(F_e = 2)$ level populations as a function of the probe laser intensity, for three cooling laser powers is shown in Figure 4. Measurements and calculations are performed for $\Delta_c = -2.7\Gamma_5$ and $I_r = 0.6$ mW/cm^2. For a given probe laser intensity, fractional $5P_{1/2}(F_e = 2)$ level population increases as the power of the cooling laser is decreased. Disagreement between measurement and theory in the case of $I_c = 5$ mW/cm^2 is understandable considering that the fluctuations in number of cold atoms in the MOT are larger at low cooling laser intensities.

The results show that measured LIF at 795 nm, which is proportional to $5P_{1/2}(F_e = 2)$ hyperfine level population excited by the probe laser, is well reproduced by the calculated ρ_{33} based on the OBEs. It is shown that it strongly depends upon the MOT parameters, such as the cooling laser detuning and power, which is not surprising since we are dealing with multi-level atoms interacting with three laser fields.

For practical purposes it is instructive to relate fractional $5P_{1/2}(F_e = 2)$ level population to the form given in equation (2), i.e. to the two-level atom excited state population. For this purpose equation (2) is fitted to the calculated ρ_{33} (as a function of probe intensity), with the effective saturation intensity, I_s^{eff}, and the constant A as free parameters of the fit. The procedure is as follows: first OBEs are solved (with I_c, Δ_c, and I_r fixed) and the dependence of ρ_{33} on probe laser intensity is obtained. Then equation (2) is fitted to the obtained data (with I_s^{eff} and A as free fit parameters), which gives the I_s^{eff} value for given MOT conditions (i.e. I_c, Δ_c, and I_r values). Dependence of the calculated I_s^{eff} on cooling laser power and detuning relevant for MOT operation (with $I_r = 0.6$ mW/cm^2) is shown in Figure 5.

Applying equation (3) to ^{87}Rb $5S_{1/2} \rightarrow 5P_{1/2}$, D1 resonance transition at 795 nm, $\Gamma/2\pi = 5.75$ MHz gives $I_s = 1.49$ mW/cm^2. This value is valid for a two-level atom interacting with a single frequency field. In the working MOT conditions two additional lasers are present (in addition to the probe laser) so the effects related to a more complex multi-level atomic system driven by multi-frequency laser fields have to be accounted for. Consequently, the obtained I_s^{eff} values depend on cooling and repumper light parameters and they are generally higher than the value calculated using equation (3). As seen in Figure 5, I_s^{eff} increases with increasing cooling laser power and decreasing the cooling laser detuning.

This is expected since the influence of the cooling laser on the $5S_{1/2}(F_g = 2) \rightarrow 5P_{1/2}(F_e = 2)$ excitation increases in these conditions.

It should be noted that I_s^{eff} is in general a function of MOT parameters, i.e. a function of three variables: I_c, Δ_c, and I_r. In typical MOT conditions $I_c > I_r$ which enables efficient cooling of atoms through the $5S_{1/2} \rightarrow 5P_{3/2}$ D2 cycling transition, while simultaneously repumper laser prevents atoms from escaping from the cooling cycle to the $5S_{1/2}(F_g = 1)$ level. I_r therefore effectively controls the population of the $5S_{1/2}(F_g = 2)$ level, and consequently also influences the population of the $5P_{1/2}(F_e = 2)$ level (ρ_{33}) induced by the probe laser. The I_s^{eff} of the probe laser must therefore depend on the repumper intensity I_r. However, this dependence is quite weak; in typical MOT working conditions calculated I_s^{eff} values (for a given I_c and Δ_c) change by less than $\pm 10\%$ when I_r is changed in the range 0.4–1.2 mW/cm^2 for the whole range of cooling laser parameters shown in Figure 5. Simultaneously, the value for constant A obtained from fit is equal to 0.18 with uncertainty of less than 10% in the whole cooling laser range shown in Figure 5. Generally, the value for A (as compared to $A = 0.5$ for two-level atom) is related to population in the $5P_{1/2}(F_e = 2)$ level which depends on both the cooling and repumper light, but in typical MOT conditions shown in Figure 5 this dependence has only a minor effect.

5 Radiation pressure force on cold Rb atoms induced by the probe beam

Radiation pressure force on cold ^{87}Rb atoms in the MOT induced by the probe laser in resonance with the $5S_{1/2}(F_g = 2) \rightarrow 5P_{1/2}(F_e = 2)$ hyperfine transition is measured and compared to the calculated force obtained from the simple model given by equations (1) and (2) using calculated I_s^{eff} as the saturation intensity I_s.

The force was measured using an approach based on imaging. The probe laser beam (exceeding the cloud size) is directed onto the cloud, inducing the displacement Δx of the cloud CM in the direction of the probe laser wavevector. In the case when probe intensity is much lower than I_s^{eff}, linear dependence of the Δx upon the probe beam intensity is expected:

$$\Delta x = \frac{1}{\kappa} \frac{\hbar k \Gamma_3 A}{I_s^{\text{eff}}} I_p. \quad (7)$$

In Figure 6 we show measured CM displacement Δx, as a function of the probe beam intensity for three magnetic field gradients. Other MOT parameters are constant during the measurements ($\Delta_c = -2\Gamma_5$, $I_c = 13$ mW/cm^2, $I_r = 0.6$ mW/cm^2), yielding $I_s^{\text{eff}} = 14.4$ mW/cm^2 for the probe laser non-cooling transition (deduced from the Fig. 5). As expected, linear dependence of the Δx upon the probe intensity is observed in all measurements. Straight lines represent best fit to the data. From equation (7) follows that the ratio of the slopes should be proportional to the inverse of the ratio of the magnetic field gradients

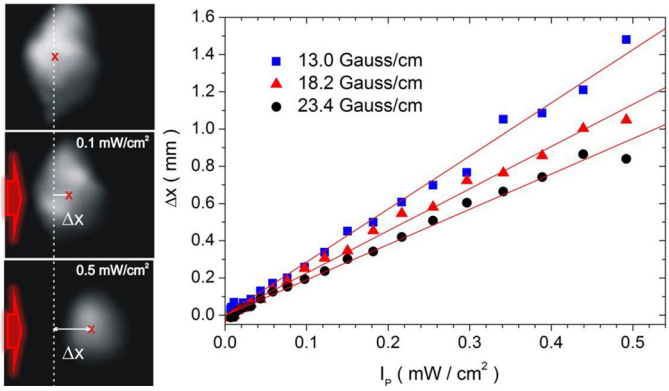

Fig. 6. Probe beam acting on the cold cloud induces the displacement Δx of the cloud CM in the direction of the probe beam propagation (left panel). Measured Δx as a function of the probe laser intensity and MOT magnetic field gradient (right panel). The straight lines are best fits to the data.

(since κ is proportional to the magnetic field gradient). Largest deviation from the expected ratio value obtained from Figure 6 is 20%, and it is mostly induced by the Δx uncertainty. Total experimental error of Δx includes the contributions from the uncertainty of MOT parameters such as cooling and repumper laser frequency, cooling laser power and magnetic field gradient.

For given MOT parameters, the probe radiative force can be obtained from the measured CM displacements Δx, using equation (4); i.e. radiative force is proportional to the measured Δx. In Figure 7 we show the measured radiative force of the probe as a function of the probe laser intensity for typical MOT parameters: 13 Gauss/cm, $\kappa = (1.3 \pm 0.2) \times 10^{-19}$ N/m, $\Delta_c = -2\Gamma_5$, $I_c = 13$ mW/cm^2, $I_r = 0.6$ mW/cm^2. Total experimental error includes contributions from the uncertainty of Δx and κ measurements. In addition to experiment, in Figure 7 we also show the calculated radiative force (red line). The calculations are based on the simple two-level model given by equations (1) and (2); in which I_s^{eff} obtained in the previous section is used as the saturation intensity I_s. The shaded area on the graph denotes force values that are within the 10% accuracy in the cooling laser intensity and detuning.

The agreement between experiment and theory is very good, confirming the applicability of our approach to the radiative force measurement and modeling even in the complex system such as cold atoms in a MOT perturbed with an additional probe laser.

6 Conclusion

We investigated experimentally and theoretically the excitation of cold ^{87}Rb atoms into the non-cooling excited state. The atoms, cooled and captured in a classical MOT, are excited by an additional probe laser tuned to the $5S_{1/2} \rightarrow 5P_{1/2}$, D1 transition. Laser induced fluorescence (LIF) was used to monitor the population in the excited state in different MOT conditions, and to investigate its

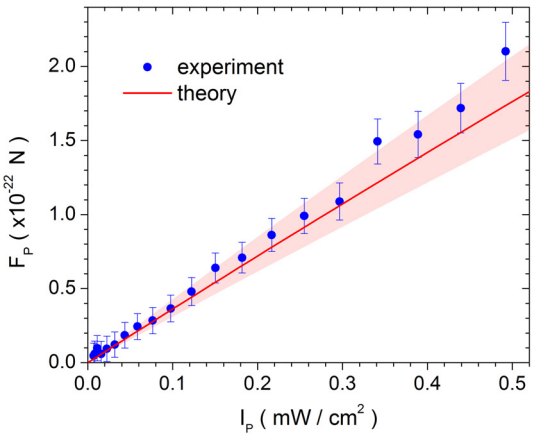

Fig. 7. Measured probe laser radiative force as a function of the probe intensity for typical MOT conditions (blue circles). Calculated radiative force (red line) with shaded area correspond to the values which are within the 10% accuracy in the cooling laser intensity and detuning.

saturation behavior for large probe laser intensities. Optical Bloch Equations (OBEs) describing the five-level atom interacting with three cw laser fields were used for the prediction of the fractional excited state populations. Agreement between experiment and theory confirms the applicability of the OBEs for describing cold atoms in the MOT.

We have used the effective saturation intensity, I_s^{eff}, of the non-cooling transition which enables modeling of the probe laser induced excited state population by a simple two-level atom model. The saturation intensity for $F_g = 2 \rightarrow F_e = 2$ D1 transition was measured and calculated. The obtained value is larger than the one calculated from equation (3) for a broad range of cooling laser parameters.

Calculated effective saturation intensity is applied for the radiative force modeling, while a technique based on imaging is used for the force measurements. Our approach of radiative force determination is accurate, simple, and robust and can be implemented in variety of experimental situations. It therefore represents a powerful tool in the research concerning all-optical manipulation of cold atoms.

Moreover, there is a number of cold atom experiments where fractional excited state population plays an important role, and therefore they could benefit from the results presented in this paper. More specifically, our work could have impact on the experiments involving the squeezed states generation, where it was lately shown that accurate determination and controlling of the excited state population induced by driving field adjusted on D1 transition is crucial for successful realization of the experiment [22].

This work was supported in part by the Unity through Knowledge Fund (UKF Grant No. 5/13), and the Ministry of Science, Education and Sports of Republic of Croatia (Project 035-0352851-2857).

References

1. M.H. Anderson, J.R. Ensher, M.R. Matthews, C.E. Wieman, E.A. Cornell, Science **269**, 198 (1995)
2. B. DeMarco, D.S. Jin, Science **285**, 1703 (1999)
3. A.G. Truscott, K.E. Strecker, W.I. McAlexander, G.B. Partridge, R.G. Hulet, Science **291**, 2570 (2001)
4. G. Kregar, N. Šantić, D. Aumiler, H. Buljan, T. Ban, Phys. Rev. A **89**, 053421 (2014)
5. T. Dubček, N. Šantić, D. Jukić, D. Aumiler, T. Ban, H. Buljan, Phys. Rev. A **89**, 063415 (2014)
6. A.M. Steane, M. Chowdhury, C.J. Foot, J. Opt. Soc. Am. B **9**, 2142 (1992)
7. H.J. Metcalf, P. van der Straten, *Laser Cooling and Trapping* (Springer-Verlag, New York, 1999)
8. D.A. Steck, *Rubidium 87 D Line Data*, http://steck.us/alkalidata
9. M.H. Shah, H.A. Camp, M.L. Trachy, G. Veshapidze, M.A. Gearba, B.D. De Paola, Phys. Rev. A **75**, 053418 (2007)
10. T.P. Dinneen, C.D. Wallace, K.Y.N. Tan, P.L. Gould, Opt. Lett. **17**, 1706 (1992)
11. G. Reinaudi, T. Lahaye, Z. Wang, D. Guéry-Odelin, Phys. Rev. A **71**, 053406 (2005)
12. E.L. Raab, M. Prentiss, A. Cable, S. Chu, D.E. Pritchard, Phys. Rev. Lett. **59**, 2631 (1987)
13. K. Jooya, N. Musterer, K.W. Madison, J.L. Booth, Phys. Rev. A **88**, 063401 (2013)
14. J. Weiner, V.S. Bagnato, S. Zilio, P.S. Julienne, Rev. Mod. Phys. **71**, 1 (1999)
15. L. Moi, G. Batignani, A. Khanbekyan, K. Khanbekyan, C. Marinelli, E. Mariotti, L. Marmugi, L. Corradi, A. Dainelli, R. Calabrese, G. Mazzocca, L. Tomassetti, P. Minguzzi, Meas. Sci. Technol. **24**, 015201 (2013)
16. K. Lindquist, M. Stephens, C. Wieman, Phys. Rev. A **46**, 4082 (1992)
17. K. Kim, K.H. Lee, M. Heo, H.R. Noh, W. Jhe, Phys. Rev. A **71**, 053406 (2005)
18. W.J. Schwenger, J.M. Higbie, Rev. Sci. Instrum. **83**, 083110 (2012)
19. C.D. Wallace, T.P. Dinneen, K.Y.N. Tan, A. Kumarakrishnan, P.L. Gould, J. Javanainen, J. Opt. Soc. Am. B **11**, 703 (1994)
20. O. Axner, J. Gustafsson, N. Omenetto, J.D. Winefordner, Spectrochim. Acta Part B **59**, 1 (2004)
21. R.W. Boyd, *Nonlinear Optics* (Academic Press, San Diego, 2003)
22. T. Horrom, S. Balik, A. Lezama, M.D. Havey, E.E. Mikhailov, Phys. Rev. A **83**, 053850 (2011)